HHS Public Access

Author manuscript

Nat Catal. Author manuscript; available in PMC 2024 July 20.

Published in final edited form as:

Nat Catal. 2023 July ; 6(7): 628–636. doi:10.1038/s41929-023-00986-5.

Enzyme-controlled stereoselective radical cyclization to arenes enabled by metalloredox biocatalysis

Wenzhen Fu[1], **Natalia M. Neris**[1], **Yue Fu**[2], **Yunlong Zhao**[1], **Benjamin Krohn-Hansen**[1], **Peng Liu**[2,*], **Yang Yang**[1,3,*]

[1]Department of Chemistry and Biochemistry, University of California, Santa Barbara, California 93106, USA

[2]Department of Chemistry, University of Pittsburgh, Pittsburgh, Pennsylvania 15260, USA

[3]Biomolecular Science and Engineering (BMSE) Program, University of California, Santa Barbara, California 93106, USA

Abstract

The effective induction of high levels of stereocontrol for free radical-mediated transformations represents a notorious challenge in asymmetric catalysis. Herein, we describe a novel metalloredox biocatalysis strategy to repurpose natural cytochromes P450 to catalyse asymmetric radical cyclisation to arenes through an unnatural electron transfer mechanism. Empowered by directed evolution, engineered P450s allowed diverse radical cyclisation selectivities to be accomplished in a catalyst-controlled fashion: $P450_{arc1}$ and $P450_{arc2}$ facilitated enantioconvergent transformations of racemic substrates, giving rise to either enantiomer of the product with excellent total turnover numbers (up to 12,000). In addition to these enantioconvergent variants, another engineered radical cyclase, $P450_{arc3}$, permitted efficient kinetic resolution of racemic chloride substrates (*S* factor = 18). Furthermore, computational studies revealed a proton-coupled electron transfer (PCET) mechanism for the radical-polar crossover step, suggesting the potential role of the haem carboxylate as a base catalyst. Collectively, the excellent tunability of this metalloenzyme family provides an exciting platform for harnessing free radical intermediates for asymmetric catalysis.

Due to their unparalleled ability to exert stereocontrol over challenging asymmetric transformations, enzymes are widely recognized as powerful tools to streamline the synthesis of chiral molecular scaffolds.[1-4] Until fairly recently, only a small set of

* pengliu@pitt.edu; yang@chem.ucsb.edu.

Author contributions

Y.Y. conceived and directed the project. W.F., N.M.N., Y.Z. and B.K.-H. designed and performed the experiments. Y.F. carried out the computational studies with P.L. providing guidance. Y.Y., Y.F. and P.L. wrote the manuscript with the input of all other authors.

Data and materials availability: All data are available in the main text and the Supplementary Information. X-ray crystal structures of **2i** and ***(R)*-3a** are available free of charge from the Cambridge Crystallographic Data Centre under reference numbers CCDC 2184585 and 2184586. Plasmids encoding $P450_{arcs}$ reported in this study are available for research purposes from Y.Y. under a material transfer agreement with the University of California Santa Barbara.

Competing interests

Y.Y., W.F., N.M.N. and Y.Z. are inventors on a patent application (UC Case No. 2023-854) submitted by the University of California Santa Barbara that covers stereoselective biocatalytic radical addition to arenes.

biochemistries from nature's catalytic repertoire has been exploited to facilitate the synthesis and manufacturing of a relatively narrow range of value-added compounds. Unfortunately, the vast majority of privileged synthetic transformations, particularly those allowing for stereoselective C—C bond formation, are not present in the state-of-the-art biocatalytic toolbox.[5] Thus, to further advance the field of biocatalysis to the next level of sophistication and applicability, it is imperative to devise and optimize synthetically useful enzyme functions which are not presently known in the biological world.[6-10]

Advances from mechanistic enzymology and structural biology have furnished invaluable insights into the molecular mechanism and structural basis of enzymatic machineries. Cross-fertilizing the fields of synthetic chemistry and enzymology, over the past decade, biocatalysis researchers initiated a campaign to repurpose and evolve natural enzymes to catalyse unnatural reactions by leveraging the synthetic versatility of common cofactors illuminated by organic and organometallic chemists.[8-10] In nature, radical enzymes[11,12] such as radical SAM enzymes[12] facilitate challenging free radical transformations. However, despite their unparalleled selectivity and intriguing mechanism, these natural radical enzymes have not yet found wide applications in synthetic chemistry and biotechnology. Very recently, new concepts and strategies in the emerging area of unnatural radical biocatalysis have led to several distinct activation modes to enable stereoselective transformations of open-shell intermediates.[10,13,14] Utilizing the strongly reducing excited-state flavin and nicotinamide cofactors, the groups of Hyster[13,15-20] and Zhao[14,21,22] pioneered an elegant photoenzymatic strategy for asymmetric radical reactions. In 2021 and 2022, by capitalizing on the innate redox activity of first-row transition-metal cofactors in common metalloproteins, our group[23,24] and the Huang group[25] advanced a metalloredox strategy to convert haem and nonhaem Fe enzymes, respectively, to catalyse stereoselective atom transfer radical reactions. Collectively, these emerging new-to-nature activation modes provide an exciting opportunity to evolve enzymes capable of imposing excellent stereocontrol over fleeting free radical intermediates, an objective that has long eluded small-molecule catalysis due to the inherent difficulties to induce asymmetry with free radical chemistry.[26-28]

To further develop and generalize the concept of metalloredox radical biocatalysis, we sought to develop a metalloenzyme-catalysed stereoselective addition of carbon-centred radicals to aromatic systems using easily available racemic α-halocarbonyls as substrates (Fig. 1).[29] In this proposed catalytic cycle (Fig. 1a), the ferrous haem protein catalyst first reacts with the alkyl halide substrate **I** to furnish a highly reactive radical species **II** via single electron transfer (SET). This incipient radical **II** subsequently adds to the aromatic ring, leading to a dearomatized radical intermediate **III**. Finally, radical-polar crossover of **III** with the ferric haem protein furnishes the final product, regenerates the ferrous protein catalyst, and completes the catalytic cycle. In this process, if the haem protein readily accommodates and transforms both enantiomeric forms of the organic halide substrate to the same radical intermediate, it would allow us to develop an enantioconvergent protocol[30] to convert racemic building blocks into enantioenriched products bearing a challenging quaternary stereocentre (Fig. 1b). Alternatively, if the haem protein catalyst effectively distinguishes the two enantiomers of the substrate and selectively converts one enantiomer,

we would be able to develop a biocatalytic kinetic resolution[31,32] to prepare enantioenriched acyclic tertiary alkyl halides, whose enantioselective synthesis remain nontrivial (Fig. 1c).[33] In asymmetric catalysis, engineering a set of structurally related yet functionally orthogonal catalysts to enable highly selective enantioconvergent transformation and kinetic resolution of the same racemic substrates remains a formidable task for both biocatalysts and small-molecule catalysts.[30] In light of the promiscuous nature of haem enzymes[34,35] as well as their ability to facilitate unnatural reactions as elegantly demonstrated by Arnold, Fasan and other researchers,[36,37] we postulated that haem-dependent radical cyclases could be evolved as a unifying platform to realize all these stereoselective processes as outlined in Fig. 1b and 1c. Herein, we describe the successful implementation of this proposal. Furthermore, our computational studies suggested a proton-coupled electron transfer (PCET) mechanism and indicated the importance of a base catalyst for the radical-polar crossover step outlined in Fig. 1a.

Results and discussion

Using α-bromo-β-amidoester **1** as the model substrate, we commenced our investigation by evaluating a panel of haem proteins and their variants, including cytochromes P450, globins and cytochromes *c* as well as our recently evolved radical cyclase mutants,[23] using intact *Escherichia coli* cells as biocatalysts (Fig. 2a, e.r. = enantiomeric ratio). We focused our initial efforts on the asymmetric synthesis of 3,3-disubstituted oxindoles, in part due to the prevalence of these structural elements in bioactive natural products and medicinal agents.[38] Among all the haem proteins we tested, although many displayed encouraging initial activities, only a handful variants from the cytochrome P450 superfamily showed moderate levels of enantioselectivity (see Supplementary Information for details). In particular, $P411_{Diane2}$ and $P411_{Diane3}$, a set of closely related variants of serine-ligated CYP102A1[39] (P450 from *Bacillus megaterium*) lacking the FAD reductase domain, which we previously engineered for enantioselective C—H amination,[40,41] exhibited good activities with opposite enantiopreferences ($P411_{Diane2}$: 58% yield, **(*S*)-2a:(*R*)-2a** = 66:34, $P411_{Diane3}$: 62% yield, **(*S*)-2a:(*R*)-2a** = 36:64).

With $P411_{Diane2}$ and $P411_{Diane3}$ as initial hits for this novel enzyme function, we set out to engineer a set of enantiocomplementary radical cyclases for the catalytic asymmetric synthesis of 3,3-disubstituted oxindoles (Fig. 2b-d). To further improve the enantioselectivity of $P411_{Diane2}$ in this unnatural radical cyclisation, by targeting amino acid residues in proximity to the haem cofactor, iterative rounds of site-saturation mutagenesis (SSM)[42] and screening were carried out. In each round of engineering, four active site residues were randomized in parallel to provide a total of four single site-saturation libraries. The selection of target residues for SSM was guided by our molecular docking studies (see Supplementary Information for details). For each SSM library, 90 clones were screened in a 96-well plate. After four rounds of directed evolution of $P411_{Diane2}$, beneficial mutations W263Q, L181M, T438G and H266L were identified, furnishing $P450_{arc1}$ (arc = aromatic radical cyclase, Fig. 2c). Based on our quantum mechanics/molecular mechanics (QM/MM) investigation,[24] the newly introduced glutamine at residue 263 likely engages the carbonyl group of the amide substrate through hydrogen bonding, thus facilitating substrate activation and enhancing enantiocontrol.[24] Under standard conditions, final variant $P450_{arc1}$ afforded

the radical cyclisation product **(*S*)-2a** in (77 ± 3)% yield, (1,330 ± 50) TTN and 96:4 e.r. (TTN = total turnover number), as determined by chiral high performance liquid chromatography (HPLC) analysis (Fig. 2b). Similarly, the enantioselectivity of $P411_{Diane3}$ could also be optimized through directed evolution. Accumulating five beneficial mutations G437A, V327P, N70S, A330F and G74P, $P450_{arc2}$ was developed to provide **(*R*)-2a** in (88 ± 1)% yield, (1,890 ± 30) TTN and 12:88 e.r. (Fig. 2d). We note that using previously developed photoenzymatic conditions, substrates bearing a small α-substituent such as **1a** provided modest enantioselectivities (78:22 e.r.) favouring the (*S*)-enantiomer.[18] Thus, the rapid engineering of enantiodivergent radical metalloenzymes $P450_{arc1}$ and $P450_{arc2}$ to access both the (*R*)- and the (*S*)-enantiomer demonstrated the power of this adaptive metalloenzyme platform to solve difficult problems in asymmetric catalysis. Additionally, steady state kinetic studies showed that our evolved enzyme $P450_{arc1}$ exhibited a 15-fold improvement in k_{cat} relative to its parent $P411_{Diane2}$, while maintaining a similar K_M value (see Table S10 for details).

Using whole *E. coli* cells harbouring newly evolved P450 radical cyclases, we next examined the substrate scope of this enantioconvergent radical C—C bond formation (Fig. 3a). Radical precursors with various α-substituents, including a methyl (**2a**), an ethyl (**2b**), a propyl (**2c**), an allyl (**2d**) and an isopropyl (**2e**) were all transformed with excellent enantioselectivities under these biocatalytic conditions, showcasing the versatility of engineered biocatalysts. Moreover, aromatic rings bearing a diverse range of *para*-substituents, including a fluorine (**2f**), a chlorine (**2g**), a bromine (**2h**), an iodine (**2i**), a methoxy (**2j**), a methyl (**2k**), an ethyl (**2l**), and an isopropyl (**2m**) all underwent radical cyclisation with excellent total turnover numbers and enantioselectivities. In addition to methyl esters (**2a**-**2m**), ethyl esters (**2n**) were also excellent substrates. Additionally, an *N*-ethyl substrate **1o** could also be successfully converted into the corresponding enantioenriched product **2o**. The absolute stereochemistry of **2i** was determined by single crystal X-ray diffraction analysis. Notably, gram-scale biotransformations could be conveniently carried out with slightly improved yield and identical enantioselectivity (**2b** and **2i**), further demonstrating the synthetic utility of these newly evolved enzymes. Furthermore, by lowering the cell density of these whole-cell biotransformations (OD_{600} = 30, 20, 10, and 5), evolved enzymes were able to provide C—C bond formation product **2b** with up to (12,000 ± 300) TTN (Fig. 2c) without lowering the yield and enantioselectivity (88% yield, 98:2 e.r.). To our knowledge, the total turnover number of the newly evolved metalloenzymes described herein represents a record high for enantioconvergent radical cyclisation to arenes.

When *meta*-substituted arene **1p** was applied, without further engineering, $P450_{arc2}$ overrode inherent substrate selectivity to furnish ***para*-2p** as the major product in 78:22 regioisomeric ratio, (1,530 ± 50) TTN and 85:15 e.r.. This result highlighted the potential of metalloenzymes to exert regiocontrol over free radical-mediated transformations. In contrast, previously developed radical cyclisation using photoredox and small-molecule Cu catalysts furnished racemic oxindole **2p** as a mixture of *para*- and *ortho*-product in ca. 1:1 ratio, slightly favouring ***ortho*-2p** (with photoredox catalyst $Ir(ppy)_3$: ***p*-2p**:***o*-2p** = 44:56, with Cu(TPA)Br: ***p*-2p**:***o*-2p** = 39:61, TPA = tris(2-pyridyl)methylamine, see Supplementary

Information for details). The non-selective nature of these reactions underscored the challenge to impose regiocontrol over radical cyclisation using conventional approaches.

We next sought to generalize this metalloenzymatic radical process to the conversion of α-chloro substrates. Gratifyingly, it was found that $P450_{arc1}$ and $P450_{arc2}$ P74G L436R F330V allowed the enantioconvergent conversion of chloride **3a** with orthogonal enantiopreferences. Under optimized reaction conditions (OD_{600} = 120), $P450_{arc1}$ gave rise to **(*S*)-2a** in 85% yield, (450 ± 60) TTN, and 94:6 e.r.. Under similar conditions with a lower cell density (OD_{600} = 30), the enantiocomplementary variant, $P450_{arc2}$ P74G L436R F330V, furnished **(*R*)-2a** in 64% yield, (1,200 ± 110) TTN, and 12:88 e.r.. Furthermore, another enzyme variant from this evolutionary lineage, $P450_{arc1}$ G438T L266H L78C V328E S332A ($P450_{arc3}$), was found to promote effective kinetic resolution of **3a**. With $P450_{arc3}$, at a conversion of 55%, (*R*)-**3a** was recovered in 94:6 e.r.. This corresponds to an *S* factor of 18 ($S = \log[(1 - c)(1 - ee)]/\log[(1 - c)(1 + ee)]$, c = conversion, $ee = ([R] - [S])/([R] + [S])$, enantiomeric excess), indicating excellent enantiodiscrimination by this kinetic resolution enzyme. Additionally, $P450_{arc3}$ allowed cyclisation product **2a** to form in 55% yield and 64:36 e.r.. Additionally, it was found that (*S*)-**3a**, the enantiomer undergoing faster radical cyclisation with $P450_{arc3}$, exhibited the same stereochemistry at the α-position as the major enantiomeric product, (*S*)-**2a**. Together, these results demonstrated the highly malleable nature of this metalloenzyme platform to effect both enantioconvergent radical cyclisation and kinetic resolution with evolutionarily related mutants.

Enzymes capable of accommodating and transforming both enantiomers of racemic substrate that are configurationally stable into the same major enantiomeric product are rare in natural biosynthetic machineries, despite a handful of recently developed new-to-nature biocatalytic enantioconvergent transformations.[15,16,18,40] To date, detailed enantioconvergent mechanisms of these unnatural biocatalytic processes remain poorly understood. With a panel of highly efficient $P450_{arc}$'s permitting the enantioconvergent transformation of both α-bromo and α-chloro substrates, we studied the evolution of the enantiomeric ratio (e.r.) of formed products and recovered substrates as a function of substrate conversion (Fig. 5).

First, when the α-bromo substrate **1b** was used, with $P450_{arc2}$ as the biocatalyst (Fig. 5a), the e.r. of product **2b** remained constant (97:3) throughout the course of the reaction, with **(*R*)-2b** as the major enantiomeric product. During this enantioconvergent transformation, as the reaction proceeded, gradual enrichment of **(*S*)-1b** in recovered **1b** was observed, showcasing kinetic resolution. With $P450_{arc2}$, this kinetic resolution occurred with low levels of enantiodiscrimination, as evidenced by a small *S* factor of (1.4 ± 0.1). Thus, although **(*R*)-1b** underwent faster conversion relative to its enantiomer **(*S*)-1b**, product **2b** derived from **(*R*)-1b** and **(*S*)-1b** exhibited identical enantiomeric ratio.

Second, when $P450_{arc1}$ was applied to transform **1b** (Fig. 5b), although the product enantiopreference was reversed to favour **(*S*)-2b**, the *same* (*R*)-enantiomer of **1b** still underwent faster conversion, similar to that with $P450_{arc2}$. Furthermore, as the reaction proceeded to higher conversions, the e.r. of product **2b** increased, indicating that the slow reacting enantiomer **(*S*)-1b** was converted to **2b** with a slightly *higher* e.r.. Similar to

$P450_{arc2}$, $P450_{arc1}$ also displayed a low kinetic resolution selectivity toward the substrate (*S* factor = 1.8 ± 0.1).

Third, starting from the α-chloro substrate **3a**, $P450_{arc1}$ furnished the same major enantiomeric product **(*R*)-2a** as that from the bromo substrate **1a** (Fig. 5c). Kinetic resolution of the substrate was also observed (*S* factor = 3.4 ± 0.5), with **(*R*)-3a** being transformed faster than **(*S*)-3a.** Using the same biocatalyst $P450_{arc1}$, the (*R*)-enantiomer of both the chloro (**3a**) and the bromo (**1a**) substrate underwent faster transformation. Interestingly, as the reaction proceeded, a slight decrease in the e.r. of **2a** was observed, suggesting that the slow-reacting **(*S*)-3a** furnished **2a** with a lower enantioselectivity. This trend is contrary to that of the bromo substrate **1b** with the same enzyme variant (*vide supra*). Together, these experiments demonstrate that for all these newly evolved enantioconvergent biocatalysts, kinetic resolution of the substrate occurs with modest selectivities, despite the ability of these biocatalysts to fully transform the racemic substrate with excellent product enantioselectivities. Furthermore, all three possible product e.r. evolution patterns, including constant e.r. (Fig. 5a), slowly increasing e.r. (Fig. 5b), and slowly decreasing e.r. (Fig. 5c), were uncovered in these studies, revealing subtle differences in enzymatic stereocontrol over enantioconvergent radical cyclisation.

To provide further insights into the reaction mechanism, we performed density functional theory (DFT) calculations using a model Fe porphyrin system, which has been used in our previous computational studies (Fig. 6).[23,24,40,41] DFT calculations showed that the Fe porphyrin catalyst remains high-spin throughout the catalytic cycle.[23,24] Due to the relatively weak C—Br bond in α-bromo-β-amidoester **1a** (BDE = 47.6 kcal/mol), the Fe-catalysed radical initiation to afford an α-carbonyl radical **4a** is highly exergonic (ΔG = −35.5 kcal/mol). With this model system bearing an anionic methoxide axial ligand, the radical initiation step prefers an outer-sphere dissociative electron transfer mechanism (DET, $\Delta G^{\ddagger}$ = 2.0 kcal/mol) over the inner-sphere electron transfer pathway (**TS1**, $\Delta G^{\ddagger}$ = 15.5 kcal/mol). The subsequent radical cyclisation to the pendant aromatic ring has an activation barrier ($\Delta G^{\ddagger}$) of 14.2 kcal/mol, indicating a sufficient lifetime for the enantioconvergent conversion of racemic starting materials via the conformational change and C—C bond rotation of radical **4a**. For the radical-polar crossover step, several proton/electron transfer pathways from the dearomatised radical intermediate **8a** to the oxindole product **2a** were considered. The most favorable mechanism features a concerted proton–electron transfer (CPET),[43] as previously studied by Mayer in a related Fe haem system,[44] where electron transfer from **4a** to the haem Fe and proton transfer from **4a** to the haem propionate occur in a concerted manner. This CPET pathway displays a low free energy barrier of 1.1 kcal/mol. Stepwise proton transfer–electron transfer (PT/ET) and electron transfer–proton transfer (ET/PT) processes are kinetically less favorable, due to the higher barriers to form the relatively unstable intermediates **11** and **12**, respectively. This finding indicates that the carboxylate group of the haem cofactor may serve as a base catalyst to facilitate the radical-polar crossover event, demonstrating the potential role of the haem cofactor as a bifunctional catalyst to greatly lower the activation barrier of radical-polar crossover. Although other basic residues in the enzyme active site may serve as the base catalyst, these DFT calculations suggest that this CPET process is more favorable, as it bypasses the

formation of high-energy intermediates resulting from stepwise electron or proton transfer. Additionally, as this CPET enables a fast and irreversible process to trap the cyclised radical intermediate **8a**, radical cyclisation (**TS2**) is expected be the enantioselectivity-determining step with the enzyme catalyst. This mechanistic scenario is consistent with KIE experiments that suggest irreversible radical cyclisation due to the kinetically facile trapping of **8a** (see Fig. S7 in the SI).

In conclusion, we have developed a unifying metalloenzyme platform for the asymmetric radical cyclisation to arenes, allowing challenging quaternary stereogenic centres to be formed with excellent enantioselectivities. Directed evolution enabled the rapid engineering of an orthogonal set of biocatalysts, allowing either enantiomeric product to be accessed via enantioconvergent radical cyclisation. Furthermore, kinetic resolution biocatalysts were also developed, giving rise to enantioenriched tertiary alkyl chlorides. For the first time, closely related biocatalysts were engineered to catalyse both enantioconvergent transformation and kinetic resolution of the same racemic substrates via a common radical mechanism. DFT calculations suggest that the radical-polar crossover event is facilitated by proton-coupled electron transfer and the C—C bond forming radical addition determines the stereoselectivity of enantioconvergent processes. Collectively, the promiscuous nature and the excellent tunability of this metalloenzyme platform highlights its potential to tackle challenging problems in asymmetric radical transformations via unnatural biocatalysis.

Methods

Expression of $P450_{arc}$ variants.

E. coli (*E. cloni* BL21(DE3)) cells carrying plasmid encoding the appropriate $P450_{arc}$ variant were grown overnight in 3 mL LB_{amp}. Preculture (1.5 mL) was used to inoculate 28.5 mL of HB_{amp} in a 125 mL Erlenmeyer flask. This culture was incubated at 37 °C and 230 rpm for 2 h. It was then cooled on ice for 20 min and induced with 0.5 mM IPTG and 1.0 mM 5-aminolevulinic acid (final concentrations). Expression was conducted at 22 °C and 150 rpm for 20 h. *E. coli* cells were then transferred to a 50 mL conical tube and pelleted by centrifugation (3,000 g, 5 min, 4 °C). Supernatant was removed and the resulting cell pellet was resuspended in M9-N buffer to OD_{600} = 5–60 (usually 15–30). An aliquot of this cell suspension (2 mL) was taken to determine protein concentration using the hemochrome assay after lysis by sonication.

Stereoselective radical cyclisation using whole *E. coli* cells harbouring $P450_{arc}$.

Suspensions of *E. coli* (*E. cloni* BL21(DE3)) cells expressing the appropriate $P450_{arc}$ variant in M9-N buffer (typically OD_{600} = 30) were kept on ice. In another conical tube, a solution of D-glucose (500 mM in M9-N) was prepared. To a 2 mL vial were added the suspension of *E. coli* cells expressing $P450_{arc}$ (typically OD_{600} = 30, 345 μL) and D-glucose (40 μL of 500 mM stock solution in M9-N buffer). This 2 mL vial was then transferred into an anaerobic chamber, where the organic substrate (15 μL stock solution (267 mM in EtOH)) was added. Final reaction volume was 400 μL; final concentrations were 10 mM substrate and 50 mM D-glucose. (Note: reaction performed with *E. coli* cells resuspended to OD_{600} = 30 indicates that 345 μL of OD_{600} = 30 cells were added, and likewise for other reaction

OD_{600} descriptions.) The vials were sealed and shaken in a Corning digital microplate shaker at room temperature and 680 rpm for 12 h.

Supplementary Material

Refer to Web version on PubMed Central for supplementary material.

Acknowledgements

This research is supported by the NIH (R35GM147387 to Y.Y. and R35GM128779 to P.L.) and the University of California, Santa Barbara (Y.Y.). We acknowledge the BioPACIFIC MIP (NSF Materials Innovation Platform, DMR-1933487) and the NSF MRSEC Program (DMR-1720256) for access to instrumentation. DFT calculations were performed at the Center for Research Computing of the University of Pittsburgh and the Extreme Science and Engineering Discovery Environment (XSEDE) supported by the National Science Foundation grant number ACI-1548562. Y.F. is an Andrew W. Mellon Predoctoral Fellow. We thank Profs. Liming Zhang (University of California Santa Barbara) and Yiming Wang (University of Pittsburgh) for critical reading of this manuscript.

References

1. Bornscheuer UT et al. Nature 485, 185–194 (2012). [PubMed: 22575958]
2. Reetz MT Angew. Chem. Int. Ed 50, 138–174 (2011).
3. Devine PN et al. Nat Rev Chem 2, 409–421 (2018).
4. Zetzsche LE, Chakrabarty S & Narayan ARH J. Am. Chem. Soc 144, 5214–5225 (2022). [PubMed: 35290055]
5. Zetzsche LE & Narayan ARH Nat Rev Chem 4, 334–346 (2020). [PubMed: 34430708]
6. Renata H, Wang ZJ & Arnold FH Angew. Chem. Int. Ed 54, 3351–3367 (2015).
7. Leveson-Gower RB, Mayer C & Roelfes G Nat Rev Chem 3, 687–705 (2019).
8. Chen K & Arnold FH Nat. Catal 3, 203–213 (2020).
9. Miller DC, Athavale SV & Arnold FH Nature Synthesis 1, 18–23 (2022).
10. Klaus C & Hammer SC Trends in Chemistry 4, 363–366 (2022).
11. Jäger CM & Croft AK ChemBioEng Reviews 5, 143–162 (2018).
12. Broderick JB, Duffus BR, Duschene KS & Shepard EM Chem. Rev 114, 4229–4317 (2014). [PubMed: 24476342]
13. Sandoval BA & Hyster TK Curr. Opin. Chem. Biol 55, 45–51 (2020). [PubMed: 31935627]
14. Harrison W, Huang X & Zhao H Acc. Chem. Res 55, 1087–1096 (2022). [PubMed: 35353478]
15. Emmanuel MA, Greenberg NR, Oblinsky DG & Hyster TK Nature 540, 414–417 (2016). [PubMed: 27974767]
16. Sandoval BA, Meichan AJ & Hyster TK J. Am. Chem. Soc 139, 11313–11316 (2017). [PubMed: 28780870]
17. Biegasiewicz KF et al. Science 364, 1166 (2019). [PubMed: 31221855]
18. Black MJ et al. Nat. Chem 12, 71–75 (2020). [PubMed: 31792387]
19. Page CG et al. J. Am. Chem. Soc 143, 97–102 (2021). [PubMed: 33369395]
20. Fu H. et al. Nature (2022).
21. Huang X. et al. Nature 584, 69–74 (2020). [PubMed: 32512577]
22. Huang X. et al. Nat. Catal 5, 586–593 (2022).
23. Zhou Q, Chin M, Fu Y, Liu P & Yang Y Science 374, 1612–1616 (2021). [PubMed: 34941416]
24. Fu Y. et al. J. Am. Chem. Soc 144, 13344–13355 (2022). [PubMed: 35830682]
25. Rui J. et al. Science 376, 869–874 (2022). [PubMed: 35587977]
26. Proctor RSJ, Colgan AC & Phipps RJ Nat. Chem 12, 990–1004 (2020). [PubMed: 33077927]
27. Mondal S. et al. Chem. Rev 122, 5842–5976 (2022). [PubMed: 35073048]
28. Sibi MP, Manyem S & Zimmerman J Chem. Rev 103, 3263–3296 (2003). [PubMed: 12914498]

29. Clark AJ Eur. J. Org. Chem 2016, 2231–2243 (2016).
30. Bhat V, Welin ER, Guo X & Stoltz BM Chem. Rev 117, 4528–4561 (2017). [PubMed: 28164696]
31. Keith John M., Larrow Jay F. & Jacobsen Eric N. Adv. Synth. Catal 343, 5–26 (2001).
32. Vedejs E & Jure M Angew. Chem. Int. Ed 44, 3974–4001 (2005).
33. Zheng Y, Zhang S, Low K-H, Zi W & Huang ZJ Am. Chem. Soc 144, 1951–1961 (2022).
34. Poulos TL Chem. Rev 114, 3919–3962 (2014). [PubMed: 24400737]
35. Phillips IR, Shephard EA & Ortiz de Montellano PR Cytochrome P450 Protocols. (Humana ; Springer, 2013).
36. Brandenberg OF, Fasan R & Arnold FH Curr. Opin. Biotechnol 47, 102–111 (2017). [PubMed: 28711855]
37. Yang Y & Arnold FH Acc. Chem. Res 54, 1209–1225 (2021). [PubMed: 33491448]
38. Zhou F, Liu Y-L & Zhou J Adv. Synth. Catal 352, 1381–1407 (2010).
39. Whitehouse CJC, Bell SG & Wong L-L Chem. Soc. Rev 41, 1218–1260 (2012). [PubMed: 22008827]
40. Yang Y, Cho I, Qi X, Liu P & Arnold FH Nat. Chem 11, 987–993 (2019). [PubMed: 31611634]
41. Mai BK, Neris NM, Yang Y & Liu PJ Am. Chem. Soc 144, 11215–11225 (2022).
42. Acevedo-Rocha CG, Hoebenreich S & Reetz MT in Directed Evolution Library Creation: Methods and Protocols (eds Gillam Elizabeth M. J., Copp Janine N., & Ackerley David) 103–128 (Springer New York, 2014).
43. Weinberg DR et al. Chem. Rev 112, 4016–4093 (2012). [PubMed: 22702235]
44. Warren JJ & Mayer JM J. Am. Chem. Soc 133, 8544–8551 (2011). [PubMed: 21524059]

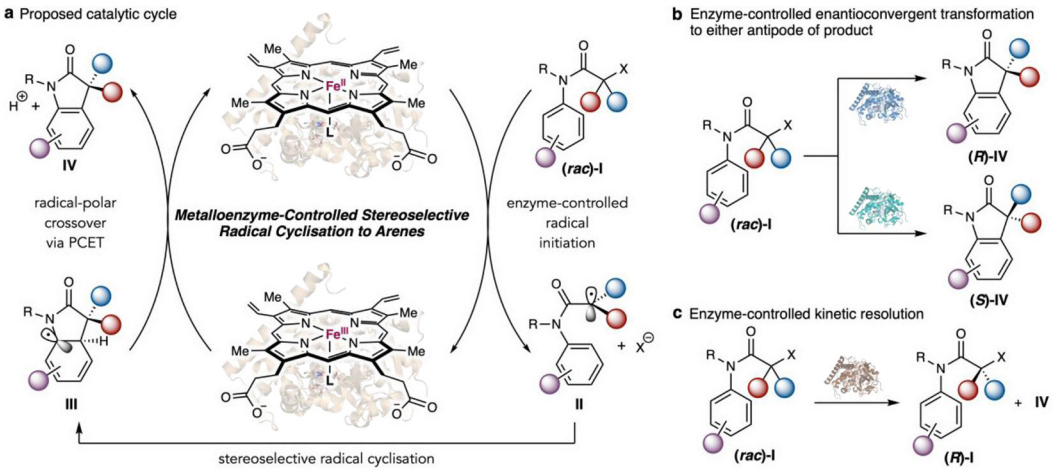

Fig. 1. A unifying metalloenzyme platform for stereoselective radical cyclisation to arenes.

a, Proposed catalytic cycle with a haemoprotein catalyst. **b**, Biocatalytic enantioconvergent radical cyclisation leading to either enantiomer of the products. **c**, Biocatalytic kinetic resolution to prepare enantioenriched tertiary alkyl halides. **L** = Fe-binding amino acid residue. In this work, **L** = serine. X = Br or Cl. PCET = proton-coupled electron transfer. Red, blue and purple spheres are generic substituents of the molecule.

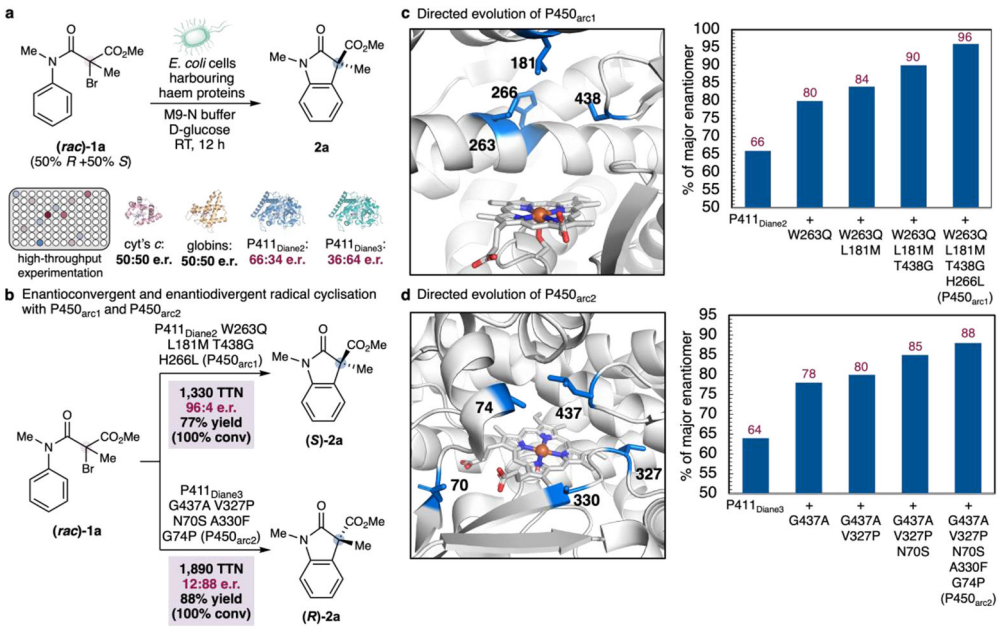

Fig. 2. Discovery and engineering of enantioconvergent P450 radical cyclases with opposite enantiopreferences.

a, Evaluation of haem protein catalysts for enantioconvergent radical cyclisation. **b**, Evolved final variants $P450_{arc1}$ and $P450_{arc2}$ as orthogonal biocatalysts for enantioconvergent radical cyclisation. **c**, Directed evolution of $P450_{arc1}$. **d**, Directed evolution of $P450_{arc2}$. Both active site illustrations were made on the basis of the crystal structure of a closely related P450 variant (PDB ID: 5UCW).

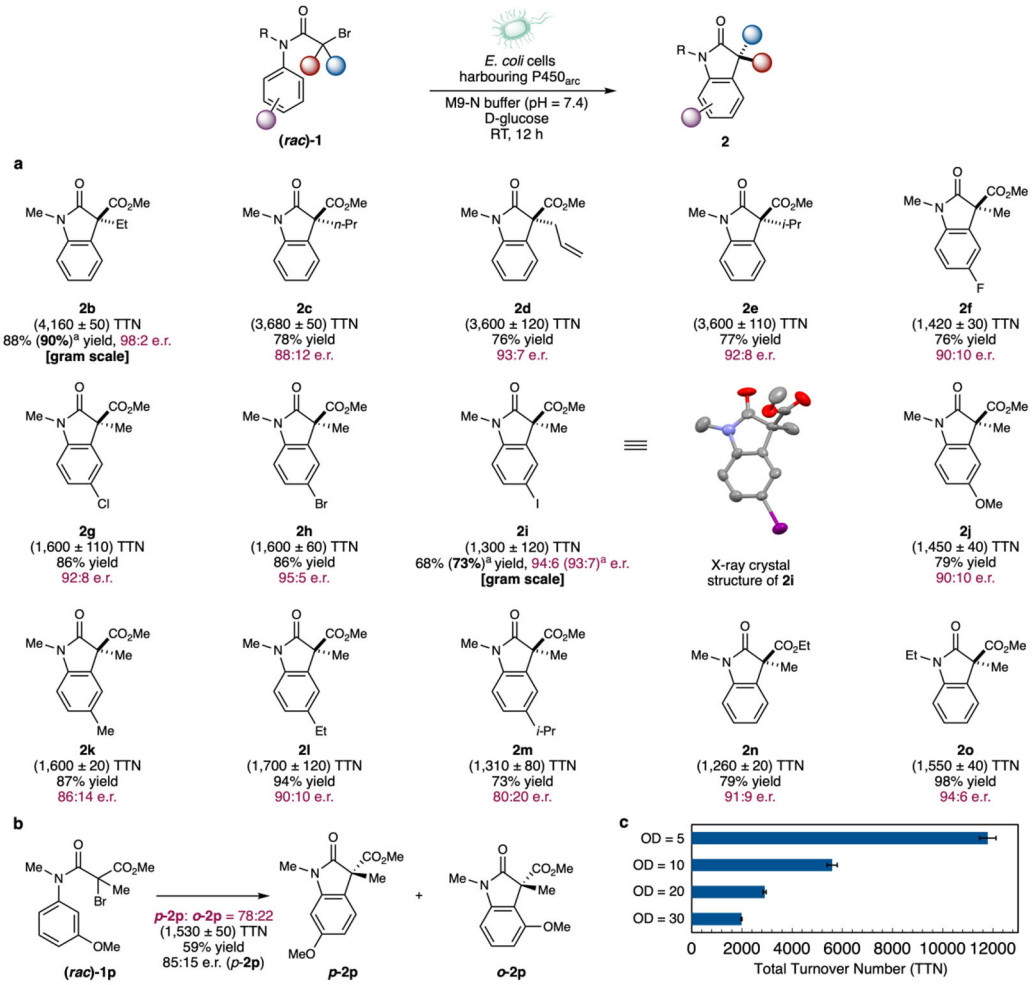

Fig. 3. Substrate scope of P450$_{arc}$-catalysed enantioconvergent radical cyclisation.

a, Substrate scope of α-bromoesters (OD_{600} = 15–35 unless otherwise noted. See Supplementary Information for details). **b**, Biocatalytic site-selective radical cyclisation of *meta*-substituted substrate **1p**. **c**, Whole-cell radical cyclisation of **1b** with high total turnover numbers (TTNs). [a]gram-scale reaction.

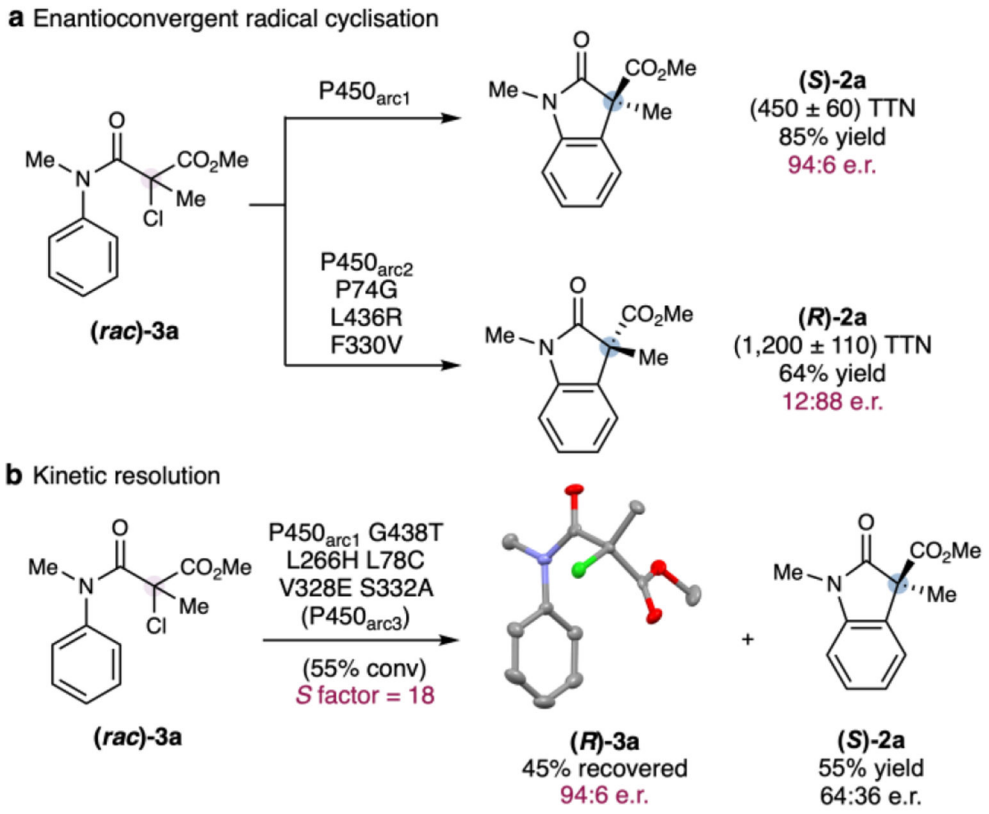

Fig. 4. P450$_{arc}$-catalysed stereoselective transformations of α-chloro substrate 3a.

a, P450$_{arc1}$ and P450$_{arc2}$ P74G L436R F330V-catalysed enantioconvergent transformation of **3a** with complementary enantiopreferences. **b**, P450$_{arc3}$-catalysed radical kinetic resolution of **3a**.

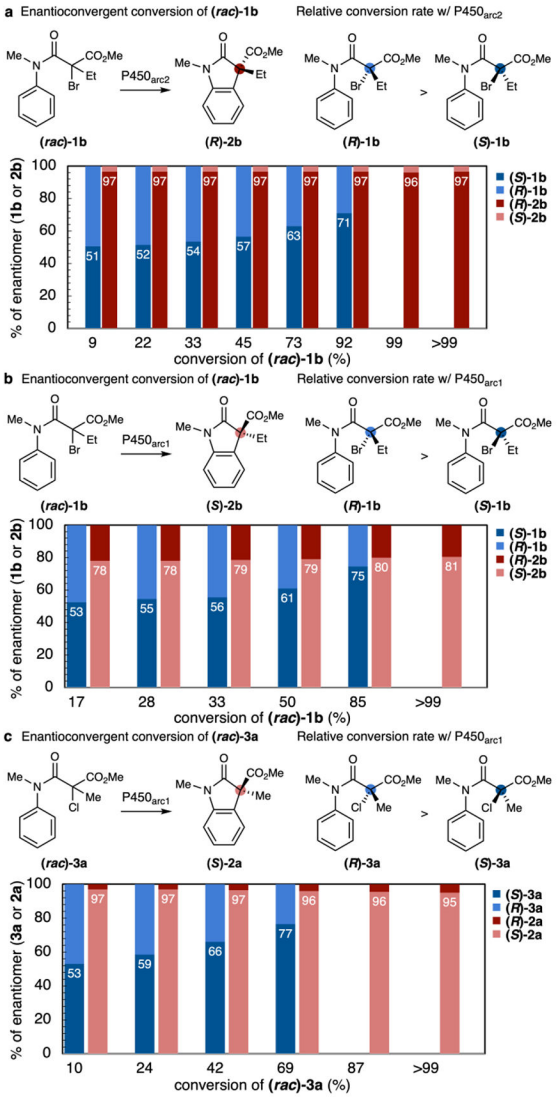

Fig. 5. Time course of P450$_{arc}$-catalysed enantioconvergent radical cyclisation processes. **a**, P450$_{arc2}$-catalysed enantioconvergent radical cyclisation of **(*rac*)-1b**. **b**, P450$_{arc1}$-catalysed enantioconvergent radical cyclisation of **(*rac*)-1b**. **c,** P450$_{arc1}$-catalysed enantioconvergent radical cyclisation of **(*rac*)-3a**.

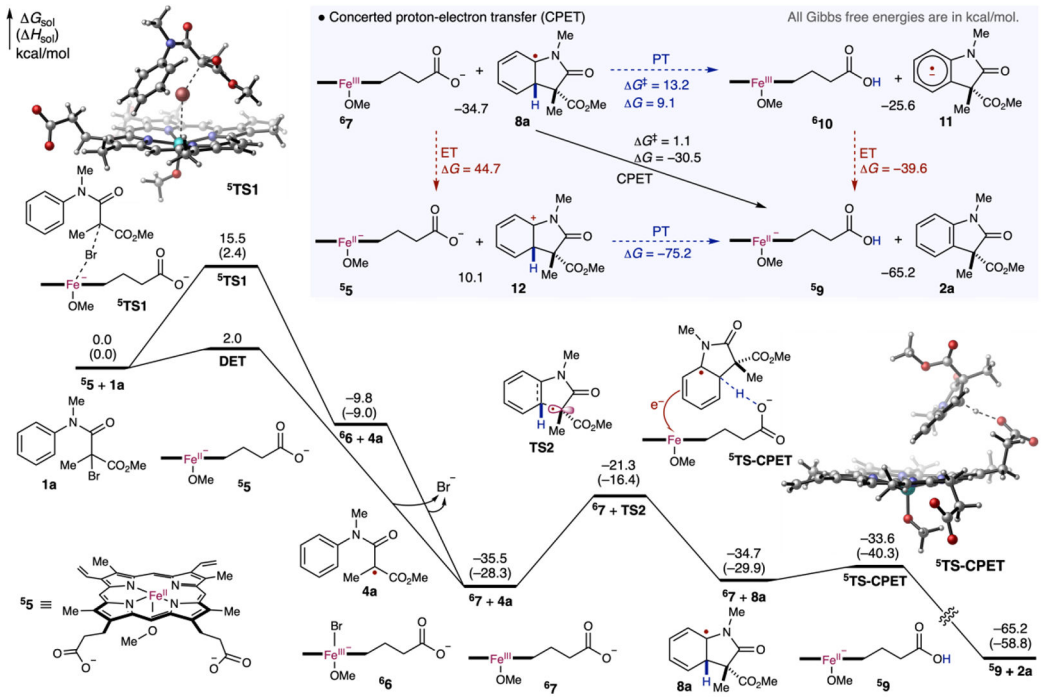

Fig. 6. Reaction energy profile of biocatalytic radical cyclisation to arenes using a model system for serine-ligated P450$_{arc}$.

Density functional theory calculations were carried out at the (U)B3LYP-D3/6-311+G(d,p)–LANL2TZ(f)/SMD(chlorobenzene)//(U)B3LYP-D3/6-31G(d)–LANL2DZ level of theory.